

LET-3D-AP: Longitudinal Error Tolerant 3D Average Precision for Camera-Only 3D Detection

Wei-Chih Hung Henrik Kretzschmar Vincent Casser
 Jyh-Jing Hwang Dragomir Anguelov

Waymo LLC

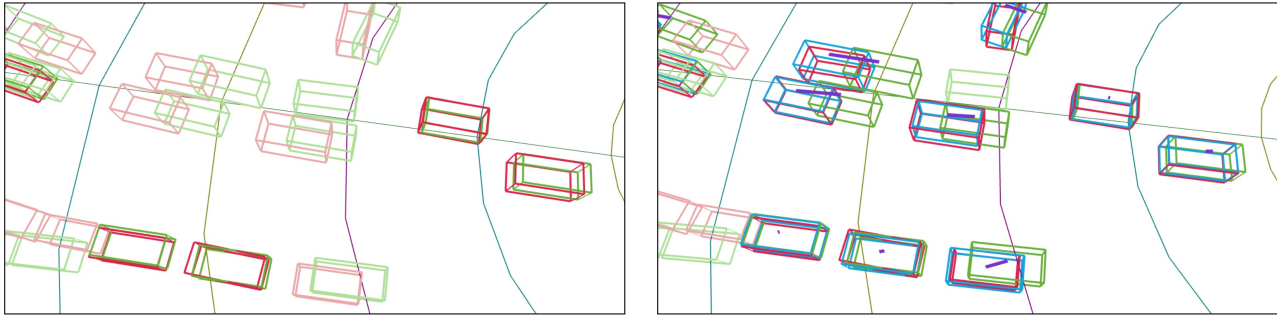


Figure 1. Evaluating camera-only 3D detections when using the popular 3D AP metric (left) and when using our proposed longitudinal error tolerant LET-3D-AP metric (right). The figures depict the bipartite matching between the detection boxes and the ground truth objects, where the unmatched prediction boxes are depicted in light green, the unmatched ground truth boxes are depicted in light red, and the matched true positive pairs are highlighted in dark green and dark red. Regular 3D AP matching shown on the left leads to hardly any valid matches owing to the longitudinal localization errors. In contrast to this, the proposed LET-3D-AP matching is more permissive by shifting the prediction boxes along the line of sight to mitigate the longitudinal localization error. We show the shifted prediction boxes in blue, which are used for computing the longitudinal error tolerant intersection over union (LET-IoU). We also show the connections between matched prediction boxes and aligned boxes with purple connectors.

Abstract

The popular object detection metric 3D Average Precision (3D AP) relies on the intersection over union between predicted bounding boxes and ground truth bounding boxes. However, depth estimation based on cameras has limited accuracy, which may cause otherwise reasonable predictions that suffer from such longitudinal localization errors to be treated as false positives and false negatives. We therefore propose variants of the popular 3D AP metric that are designed to be more permissive with respect to depth estimation errors. Specifically, our novel longitudinal error tolerant metrics, LET-3D-AP and LET-3D-APL, allow longitudinal localization errors of the predicted bounding boxes up to a given tolerance. The proposed metrics have been used in the Waymo Open Dataset 3D Camera-Only Detection Challenge. We believe that they will facilitate advances in the field of camera-only 3D detection by providing more informative performance signals.

1. Introduction

Detecting objects such as vehicles in 3D space is a fundamental task in autonomous driving. While LiDAR-based object detection [8, 11, 13, 17, 19, 21, 28] has been studied extensively in recent years with impressive results, reliable camera-based 3D object detection remains a challenging and active area of research [3, 5, 12, 14–16, 18, 23–27].

According to common metrics, LiDAR-based detectors outperform camera-based detectors by a large margin, suggesting that camera-based object detectors fail to detect many relevant objects in the scene. However, a careful evaluation of the failure cases reveals that many camera-based detectors identify objects reasonably well. The issue is rooted in these detectors often poorly estimating depth, that is, how far away objects are from the camera. Common metrics, such as the popular 3D AP metric, rely on the intersection over union (IoU) to associate the predicted bounding boxes with the ground truth bounding boxes. As a result of this, they may treat otherwise reasonable predictions that suffer from

these longitudinal localization errors as false positives and false negatives, leading to lower and less informative scores.

We therefore propose a variant of the 3D AP metric that is designed to be more permissive with respect to depth estimation errors. Our novel longitudinal error tolerant metrics, LET-3D-AP and LET-3D-APL, allow longitudinal localization errors up to a given tolerance. Specifically, we define the longitudinal error to be the object localization error along the line of sight between the camera and the ground truth bounding box. The maximum longitudinal error that our metric tolerates for a prediction to be associated with a ground truth object is an adjustable percentage of the distance between the camera and the ground truth object.

We define the longitudinal affinity of a prediction with respect to a ground truth object to describe how close the predicted object is to a ground truth object within the tolerance range. We consider all pairs of predicted bounding boxes and ground truth objects. For each pair, we correct the longitudinal localization error by shifting the predicted bounding box along the line of sight between the camera and the center of the predicted bounding box. This minimizes the distance between the centers of the predicted bounding box and the ground truth object. We then use the resulting corrected bounding box to compute the IoU, which we refer to as the longitudinal error tolerant IoU (LET-IoU). The precision and recall values are then computed by performing a bipartite matching with weights based on the longitudinal affinity and the LET-IoU values.

Finally, we define two longitudinal error tolerant metrics, LET-3D-AP and LET-3D-APL. First, the metric LET-3D-AP is the average precision based on the counts of TP 's, FP 's, and FN 's. Note that this metric does not penalize any corrected longitudinal localization errors. This metric is therefore comparable to the original 3D AP metric, but with more tolerant matching criteria. In contrast to this, the metric LET-3D-APL penalizes longitudinal localization errors by scaling the precision using the longitudinal affinity.

We evaluate the proposed metrics on the Waymo Open Dataset [20]. Our experimental results suggest that they reflect object detection performance in a more meaningful way. Specifically, we observe that our metrics reward many reasonable detections that are penalized when using regular metrics. Figure 1 visually compares 3D AP to our proposed metrics.

2. Related Work

Following popular 2D detection benchmark datasets, such as PASCAL VOC [6] and COCO [9], most 3D object detection benchmark datasets for autonomous driving rely on the metric 3D AP to evaluate detection performance based on the intersection over union (IoU), either in 3D or in a bird's eye view (BEV), with predefined IoU thresholds. For example, the KITTI dataset [7] and the Waymo Open Dataset [20]

follow the PASCAL VOC evaluation and adopt 3D IoU as the main matching function. The Waymo Open Dataset proposes to use a heading accuracy weighted AP, referred to as APH, as the primary metric to penalize incorrect heading prediction. NuScenes [4] uses the center distance between predicted objects and ground truth objects as the true positive matching criterion and proposes a set of true positive metrics to quantify other errors, including localization, scale, and orientation.

While LiDAR-based detectors [8, 11, 13, 17, 19, 21, 28] remain the most popular methods for 3D object detection for autonomous driving, monocular camera-based 3D object detection has been gaining traction in recent years. Methods can be roughly categorized into two groups: those that predict 3D box attributes based on 2D detections [3, 5, 12, 18, 23, 26, 27] and those that predict 3D feature maps in bird's eye view (BEV) [14, 24, 25] or in voxel space [15, 16]. These methods then predict the detections by applying 3D detection heads to the feature maps. Accurate monocular depth estimation is essential to these methods. Since monocular depth estimation is intrinsically an ill-posed problem, however, it is difficult for camera-based methods to accurately estimate the depth that corresponds to the objects, resulting in longitudinal localization errors that lead to reduced 3D AP scores when compared to LiDAR-based methods.

As pointed out by Ma *et al.* [10], the performance of monocular camera 3D detection methods can be greatly improved when their longitudinal localization errors are mitigated by using ground truth depth or localization. This is why we are proposing longitudinal error tolerant (LET) metrics for evaluating camera-only 3D detection methods.

3. Average Precision for Object Detection

Average precision (AP) is a common metric to quantify the performance of a classifier as given by a precision-recall curve. To apply average precision to the task of object detection, we need to define a notion of true/false positives/negatives for a set of detections. It is common practice to treat a detection as a true positive if it is *matched* with a ground truth object and as a false positive if it is not matched with a ground truth object. Many popular metrics rely on the intersection over union (IoU) for determining how to match the predictions with the ground truth objects.

Average Precision for 2D and 3D object detection is commonly calculated as follows:

1. For all detection and ground truth pairs, calculate the intersection over union (IoU) between the corresponding two bounding boxes.
2. Compute bipartite matching, matching detections with ground truth objects only if the IoU surpasses a certain threshold. Count matched pairs as true positives TP ,

non-matched ground truth objects as false negatives FN , and non-matched detections as false positives FP .

3. Compute the recall r and the precision p , leading to $r = TP/(TP + FN)$ and $p = TP/(TP + FP)$.
4. Calculate a precision-recall (PR) curve $p(r)$ by varying the detection score cutoffs.
5. Calculate the average precision AP as $\int_0^1 p(r)$.

Our intention is to follow the 3D AP metric as closely as possible, while modifying the matching criterion for true positives by providing a more permissive association between predicted objects and ground truth objects. This allows us to capture detections with erroneous localization.

4. Longitudinal Error Tolerant 3D Average Precision

The 3D AP metric relies on the intersection over union to match prediction boxes with ground truth boxes. Therefore, prediction boxes that have no overlap with the corresponding ground truth boxes will be treated as false positive detections. However, these predictions may still contribute valuable information to the decision making of an autonomous driving system. We therefore propose a metric that rewards such detections.

Figure 1 (left) depicts the bipartite matching between the detection boxes of a camera-only detector and the ground truth objects of an example scene when using regular 3D-IoU for matching. Note how most prediction boxes in the scene are not matched with any ground truth boxes and are therefore treated as false positives. In contrast to this, our proposed metrics capture many more matches between prediction boxes and ground truth boxes (right).

Our proposed metrics are inspired by the following objectives:

- Given a model of an assumed localization error distribution, design a new matching criterion so that a predicted bounding box may still match with a target ground truth bounding box even when they do not overlap in terms of IoU.
- Design a new bipartite matching cost function that takes the localization, shape, and heading errors into account so that frame-level matching can be properly calculated by the Greedy/Hungarian Matcher.
- Design a penalty term to penalize detections that can only be matched with the ground truth when using the localization noise-tolerant matching.

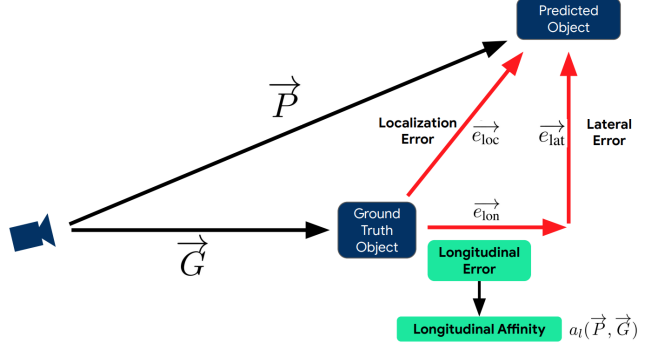


Figure 2. **Breakdown of the localization error.** We decompose the 3D detection localization error into a lateral error and a longitudinal error. We find that the longitudinal error is more prominent in camera-only 3D detection. We therefore propose longitudinal error tolerant (LET) metrics that are more permissive with respect to the longitudinal localization error.

4.1. Localization Errors in Camera-Based 3D Detection

Given a ground truth bounding box with center $\vec{G} = [x_g, y_g, z_g]$ and a predicted bounding box with center $\vec{P} = [x_p, y_p, z_p]$ such that the origin $[0, 0, 0]$ is the camera location, and $\vec{u} = [1, 0, 0]$ is the normalized direction of the principal axis, that is, all 3D location vectors are in the camera frame. We define the localization error as the vector

$$\vec{e}_{\text{loc}} = \vec{P} - \vec{G}. \quad (1)$$

We decompose the localization error into two components:

1. The longitudinal error \vec{e}_{lon} is the error along the line of sight from the center of the prediction bounding box to the center of the ground truth bounding box, giving $\vec{e}_{\text{lon}} = (\vec{e}_{\text{loc}} \cdot \vec{G}) \times \vec{u}_G$, where $\vec{u}_G = \vec{G}/|\vec{G}|$ is the unit vector along the line of sight to the ground truth given by \vec{G} .
2. The lateral error \vec{e}_{lat} is the distance between the center of the predicted bounding box P and the line of sight from the sensor to the center of the ground truth bounding box G . In other words, the lateral error is the shortest distance from the center of the predicted box to any point on the line of sight, leading to $\vec{e}_{\text{lat}} = \vec{e}_{\text{loc}} - \vec{e}_{\text{lon}}$.

Figure 2 illustrates the error terms. We observe that localization errors in terms of object centers tend to have the following attributes for camera-based 3D detectors:

- Localization errors tend to be the most pronounced along the line of sight. This is because localization errors mostly stem from imperfect depth estimation. Therefore, we assume that the standard deviation of the longitudinal error, \vec{e}_{lon} , is proportional to the distance

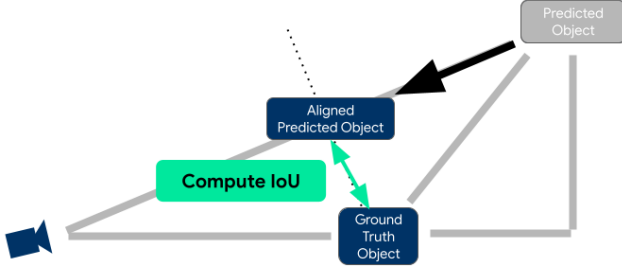


Figure 3. **Computing LET-IoU.** Given a predicted object and a ground truth object to be matched with, we move the predicted object along the line of sight to obtain minimal distance to the ground truth center. We then compute the LET-IoU as the 3D-IoU between the aligned predicted object and the ground truth object.

between the sensor and the center of the ground truth bounding box, \vec{G} .

- The lateral error, \vec{e}_{lat} , of a camera-only detection is the result of an imperfect estimation of the object center on the camera image plane. Since the size of the bounding box projected onto the camera plane is inversely proportional to the range to a given ground truth, G , the standard deviation of the center estimation error in pixels, $\sigma(|e_{\text{cam}}^-|)$, is also inversely proportional to the range of a given ground truth \vec{G} , that is, $\sigma(|e_{\text{cam}}^-|) \propto 1/|\vec{G}|$. The actual lateral error in 3D space, however, is scaled by the range projection, that is, $\vec{e}_{\text{lat}} = |\vec{G}| \times \sigma(|e_{\text{cam}}^-|)$. Therefore, the standard deviation of the lateral error is independent of the range of the ground truth object, that is, $\sigma(|e_{\text{lat}}^-|) = |\vec{G}| \times \sigma(|e_{\text{cam}}^-|) = |\vec{G}| \times k/|\vec{G}| = k$, where k is an arbitrary constant.

We therefore only introduce a tolerance for the longitudinal localization errors.

4.2. Longitudinal Affinity

We propose a scalar value, longitudinal affinity $a_l(\vec{P}, \vec{G})$, to determine the scores for matching predicted bounding boxes with ground truth bounding boxes given a tolerance for the longitudinal error. Specifically, the longitudinal affinity, whose value is in $[0.0, 1.0]$, estimates how well the centers of a predicted bounding box and the ground truth bounding box align. Given the longitudinal error, e_{lon}^- , between a pair of prediction and ground truth, we define the longitudinal affinity based on the following hyperparameters:

- `longitudinal_tolerance_percentage` T_l^p : The maximum longitudinal error e_{lon}^- is expressed as a percentage T_l^p of the range to the ground truth G . For example, with $T_l^p = 0.1$, that is a 10% tolerance, and a ground truth object that is 50 meters away, that is $|\vec{G}| = 50$, the longitudinal tolerance is 5 meters.

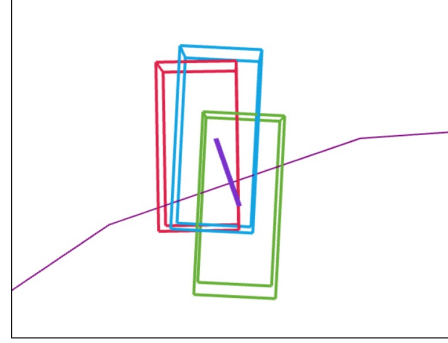


Figure 4. **An example of a matched detection using LET-IoU.** The green box denotes the detection, the red box denotes the ground truth, and the blue box denotes the longitudinal aligned detection as stated in section 4.3. We also show the connections between matched prediction boxes and aligned boxes with purple connector.

- `min_longitudinal_tolerance_meter` T_l^m : When a ground truth object is close to the sensor origin, the percentage-based tolerance results in a small matching region. This parameter controls the tolerance for near range objects.

Finally, we define the longitudinal affinity $a_l(\vec{P}, \vec{G})$ between a detection box with center \vec{P} and a ground truth box with center \vec{G} as:

$$a_l(\vec{P}, \vec{G}) = 1 - \min\left(\frac{|e_{\text{lon}}^-(\vec{P}, \vec{G})|}{T_1}, 1.0\right), \quad (2)$$

where $T_l = \max(T_l^p \times |G|, T_l^m)$.

4.3. LET-IoU: Logitudinal Error Tolerant IoU

The longitudinal affinity captures the longitudinal error of a prediction based on the center of the predicted bounding box and the center of the ground truth bounding box. To determine whether a prediction can be associated with a ground truth, we also want to take into account the shape, size, and heading error. When relying on the regular 3D AP, this is only captured by 3D IoU. We propose LET-IoU, where IoU is calculated between the ground truth bounding box and the prediction bounding box after compensating for the longitudinal error. Specifically, we mitigate the longitudinal error of the prediction by aligning its center along the line of sight with the ground truth.

Given a ground truth with center \vec{G} and a prediction with center \vec{P} , we move the center location of the prediction box along the line of sight so that its center has the closest distance to the ground truth center. In other words, the center of the aligned prediction is the projection of the ground truth center \vec{G} onto the line of sight from the sensor to the

prediction object, leading to

$$P_{\text{aligned}} = (\vec{G} \cdot \vec{u}_P) \times \vec{u}_P, \quad (3)$$

where $\vec{u}_P = \vec{P}/|\vec{P}|$ is the unit vector along the line of sight to prediction center \vec{P} . Finally, we obtain the LET-IoU by calculating the typical 3D IoU between the aligned prediction box P and the target ground truth box G , giving

$$\text{LET-IoU}(P, G) = \text{3D-IoU}(P_{\text{aligned}}, G), \quad (4)$$

where P_{aligned} is the prediction box with aligned center P_{aligned} . See Figure 3 for an illustration.

Note that for simplicity, this function does not assume that the longitudinal error is within a given tolerance. In the final metrics computation, LET-IoU will only be calculated on pairs with non-negative longitudinal affinity, where $a_l > 0$.

Figure 4 shows that the prediction (green) is aligned to the target ground truth (red), where the 3D IoU is computed between the aligned prediction (yellow) and the ground truth, resulting in 0.7 LET-IoU.

4.4. Bipartite Matching with Longitudinal Error Tolerance

To calculate the precision and recall values, detection metrics need to perform a bipartite matching between the prediction set and the ground truth set. Most bipartite matching algorithms involve computing an association weight matrix $W \in \mathcal{R}^{N_P \times N_G}$, where N_P and N_G are the numbers of detections and ground truth objects. The objective is to maximize the summed weights among all the matched pairs. We may take into consideration the longitudinal error, the shape error, and potentially the heading error.

The typical matching weight function in 3D AP computes the IoU between a prediction box and a ground truth box with an IoU threshold T_{iou} :

$$W(i, j) = \begin{cases} \text{IoU}(P(i), G(j)), & \text{if } \text{IoU}(P(i), G(j)) > T_{\text{iou}} \\ 0, & \text{otherwise} \end{cases}, \quad (5)$$

where P and G are the prediction box set and ground truth box set for a single frame. However, in our setting, there are two affinity terms to be considered: longitudinal affinity a_l and LET-IoU. As a result, we propose to calculate the bipartite matching weight where both terms are taken into account:

$$W(i, j) = \begin{cases} a_l \times \text{LET-IoU}, & \text{if } a_l > 0 \\ & \text{and LET-IoU} > T_{\text{iou}}, \\ 0, & \text{otherwise} \end{cases}, \quad (6)$$

where we omit the function input terms $(P(i), G(j))$ of a_l and LET-IoU for simplicity. This allows us to take the shape and heading error into account while prioritizing the detections that have higher longitudinal affinity.

After computing the matching weight matrix, we run a bipartite matching method (Greedy or Hungarian) to compute the matching results, including matched pairs (true positives / TP), non-matched predictions (false positives / FP), and non-matched ground truths (false negatives / FN).

4.5. LET-3D-AP and LET-3D-APL

4.5.1 LET-3D-AP: Average Precision with Longitudinal Error Tolerance

Once the matching results are finalized, each matched prediction will be counted as a true positive (TP). A prediction without matching ground truth is counted as a false positive (FP). If a ground truth is not matched with any prediction, the ground truth is counted as a false negative (FN). Then the precision $p = |TP|/(|TP| + |FP|)$ and recall $r = |TP|/(|TP| + |FN|)$ can be calculated. After computing the precision and recall values for detection subsets with different score cutoffs, a PR curve can be obtained. Finally, the LET-3D-AP is calculated from the average precision of the PR curve:

$$\text{LET-3D-AP} = \int_0^1 p(r) dr, \quad (7)$$

where $p(r)$ is the precision value at recall r .

Here, we do not penalize depth errors when computing the PR curve, even though we may have had to adjust some predictions to compensate for their depth errors. This provides a number to compare with existing 3D AP but with a more tolerant matching criterion.

4.5.2 LET-3D-APL: Longitudinal Affinity Weighted LET-3D-AP

Here, we penalize those predictions that do not overlap with any ground truth, that is, that only match a ground truth bounding box owing to the above-mentioned center alignment. We penalize these predictions by using the longitudinal affinity, $a_{loc}(\vec{P}, \vec{G})$, proposed above. To this end, we propose a weighted variant of precision values.

Though the number of true positives $|TP|$ is used both in the precision and recall computation, they represent different ideas. In precision calculation, $|TP_P|$ means the number of matched predictions. While in the recall calculation, $|TP_G|$ means the number of matched ground truths. As a result, we rewrite the precision and recall as

$$\text{Precision} = \frac{|TP_P|}{|TP_P| + |FP|} \quad (8)$$

$$\text{Recall} = \frac{|TP_G|}{|TP_G| + |FN|} \quad (9)$$

to emphasize the difference between the prediction accumulator and the ground truth accumulator.

In the precision computation, we traverse through the predictions to accumulate the FP 's and TP 's. For any unmatched prediction, it only contributes to the FP -accumulators with 1.0. However, for a matched prediction P with LET matching criteria with respect to a ground truth \vec{G} , it contributes to TP -accumulator with the quantity of $a_l(\vec{P}, \vec{G})$ and also contributes to the FP -accumulator with the quantity of $1 - a_l(\vec{P}, \vec{G})$. Essentially, we distribute part of the TP -accumulator to the FP -accumulator based on the longitudinal affinity. Then, the soft TP - and FP -accumulators are:

$$|TP_P| = \sum_{\text{matched } P} a_l(\vec{P}, \vec{G}) \quad (10)$$

$$|FP| = \sum_{\text{matched } P} (1 - a_l(\vec{P}, \vec{G})) + \sum_{\text{unmatched } P} 1.0 \quad (11)$$

The soft precision can then be computed as:

$$Prec_L = \frac{|TP_P|}{|TP_P| + |FP|} \quad (12)$$

$$= \frac{\sum_{\text{matched } P} a_l(\vec{P}, \vec{G})}{\sum_{\text{matched } P} a_l(\vec{P}, \vec{G}) + \sum_{\text{matched } P} (1 - a_l(\vec{P}, \vec{G})) + \sum_{\text{unmatched } P} 1.0} \quad (13)$$

$$= \frac{\sum_{\text{matched } P} a_l(\vec{P}, \vec{G})}{\sum_P 1.0} \quad (14)$$

$$= \frac{\sum_{\text{matched } P} a_l(\vec{P}, \vec{G})}{\sum_{\text{matched } P} 1.0} \cdot \sum_{\text{matched } P} \frac{1.0}{\sum_P 1.0} \quad (15)$$

$$= \bar{a}_l \cdot Precision, \quad (16)$$

which results in a mean longitudinal affinity weighted precision point.

For the recall computation, we propose to not weight the TP_G since the ground truth does get matched, and there is no reason to penalize the metric twice. As a result, the precision values are discounted by the multiplier \bar{a}_l , which is the average longitudinal affinity of all the matched predictions that was treated as TP .

Finally, the LET-3D-APL can be calculated with the longitudinal affinity weighted PR curve:

$$LET\text{-}3D\text{-}APL = \int_0^1 p_L(r) dr = \int_0^1 \bar{a}_l \cdot p(r) dr, \quad (17)$$

where $p_L(r)$ is the longitudinal affinity weighted precision value, and $p(r)$ is the precision value at recall r . Note that the weight $a_l(\vec{P}, \vec{G})$ depends on the specific score cutoff at the PR point and therefore cannot be taken out of the integral.

5. Experimental Results

In this section, we provide a quantitative analysis of the proposed LET metrics against both LiDAR-based and Camera-only 3D detectors.

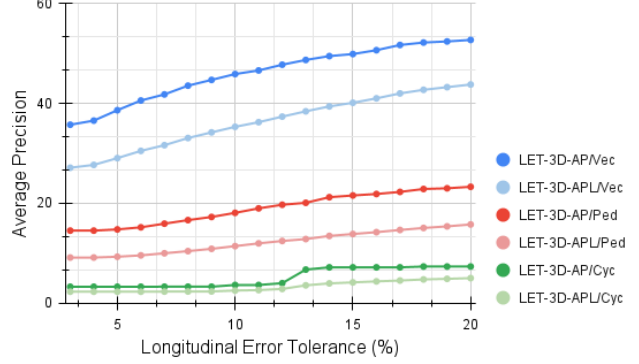


Figure 5. **LET metrics with different longitudinal error tolerance values.** We show the LET-3D-AP and LET-3D-APL of the Camera-Only Detector on the Waymo Open Dataset. With higher tolerance, the metrics become higher due to more detections are matched with ground truth objects. The metrics saturated after 15% for the chosen method. However, the actual tolerance value should be set according to the tolerance of downstream task to provide a more informative metric.

5.1. Evaluation Dataset and Baseline Methods

To verify the proposed LET metrics, we evaluate two representative 3D detectors trained on the Waymo Open Dataset [20] (WOD) and report different metrics proposed in this work:

- **LiDAR Detector:** A LiDAR-based 3D detector trained on the WOD training set with range images as input.
- **Camera-Only Detector:** A Camera-Only Monocular 3D detector trained on the WOD training set. The LiDAR range images are used in the training process for camera pixel depth estimation. During inference, only camera images are used. We train the detector on all 5 camera views provided in the dataset and simply merge the detection results of all views with the extrinsic information of the cameras.

5.2. Comparisons of Longitudinal Tolerance Values

The main hyper-parameter of the proposed metrics is the longitudinal tolerance percentage T_l^p , which establishes a relative threshold on allowed longitudinal error, as a function of ground truth depth. We show the performance of the **Camera-Only Detector** with different tolerance values in Figure 5, where both LET-3D-AP and LET-3D-APL are shown for three classes: vehicles (Vec), pedestrians (Ped), and cyclists (Cyc).

As shown in Figure 5, the higher longitudinal error tolerance always yield higher LET-3D-AP and LET-3D-APL. This is due to more ground truth objects are matched with detections, resulting in improved average precision at each score cutoff point.

Method	T_{IoU}	3D AP (%)	LET-3D-AP (%)	LET-3D-APL (%)	mLA (APL / AP)
LiDAR Detector	0.7	68.6	71.4	68.1	0.953
	0.5	76.3	77.6	73.7	0.950
	0.3	86.5	87.7	83.1	0.948
Camera-Only Detector	0.7	3.1	23.0	16.0	0.696
	0.5	20.5	43.3	33.9	0.783
	0.3	31.3	45.5	30.7	0.674

Table 1. **Comparisons of 3D AP, LET-3D-AP, and LET-3D-APL.** We evaluate both the LiDAR Detector and the Camera-Only Detector on the Waymo Open Dataset and report the 3D AP, and the proposed LET-3D-AP, LET-3D-APL. The results show that when detections are localized accurately, LET-3D-AP/LET-3D-APL is close to the typical 3D AP. But when the longitudinal error is represented in the case of Camera-Only Detector, the proposed LET metrics can produce more informative feedback.

The choice of the longitudinal tolerance depends on the requirements of the downstream modules, e.g. tracking or behavior prediction, especially for an autonomous driving system. Users can also sweep the tolerance values to gain more understanding of the behavior and error patterns of the target 3D detector. However, note that the proposed method may produce implausible associations when the tolerance value is set too high.

Since `min_longitudinal_tolerance_meter` is introduced to handle extremely close range detections, we set it to 0.5 meters throughout our experiments, and we heuristically find that it produces reasonable association results in the very near range.

5.3. LET-3D-AP vs 3D AP

We compare the proposed LET-3D-AP and LET-3D-APL with the conventional 3D AP on the two baselines: LiDAR Detector and Camera-Only Detector. The longitudinal tolerance is set to 10%, and we only report the metrics of the vehicle class in Table 1 under 0.3, 0.5, and 0.7 (LET-) IoU thresholds.

In Table 1, we show that LET-3D-AP is only slightly higher than the 3D AP with 1.2%-2.8% difference for the LiDAR based detector due to the small amount of additional detections being matched with ground truth objects with more localization error tolerance. Also, due to the accuracy of LiDAR range estimates, the boxes are really accurate, resulting in minimal difference between LET-3D-AP and LET-3D-APL. Only 5% of the allowed longitudinal tolerance is used on average.

The LET-3D metrics results of the Camera-Only Detector in Table 1 exhibit a much larger gap to the 3D AP baseline. For the 0.7 IoU threshold, which is a typical value for vehicle 3D AP detection in several benchmark datasets, the LET-3D-AP increases from 3.1% to 23.0%. Compared to the LiDAR detector, the drop off between LET-3D-AP and LET-3D-APL is much larger, demonstrating much higher longitudinal error among the true positive examples.

5.4. 3D Camera-Only Detection Challenge

The proposed metrics LET-3D-APL and LET-3D-AP serve as the primary and secondary metrics for the 2022 Waymo Open Dataset 3D Camera-Only Detection Challenge [1]. In this challenge, we set the longitudinal error tolerance to 10%, which is based on the observation that recent monocular depth estimation methods are usually within less than 10% relative depth error, as suggested by the KITTI depth estimation leaderboard [22]. We also set the minimum longitudinal error tolerance to 0.5m. We set the pre-specified IoU thresholds for vehicles, pedestrians and cyclists to 0.5, 0.3 and 0.3, respectively. We provide an implementation of the metrics in the Waymo Open Dataset code repository [2]. We provide a leaderboard with a detailed breakdown in terms of range and different cameras on the Challenge website [1].

We show the detailed metrics of the winning methods in Table 2. All methods are evaluated on the Camera-Only test set which consists of 80 multi-camera sequences. We report 3D AP, LET-3D-AP, LET-3D-APL, and mean longitudinal affinity (mLA) for all class and range breakdowns. Note that the 3D AP metrics are computed with the above IoU thresholds rather than the original 0.7, 0.5, 0.5 thresholds used in the Waymo Open Dataset 3D Detection Challenge.

As shown in Table 2, LET-3D-AP values are consistently higher than 3D AP values since more detections are matched with ground truth objects with additional longitudinal tolerance. The difference is especially pronounced for small objects like pedestrians, as well as far-away objects. We also report the mean longitudinal affinity values to show the difference between LET-3D-AP and LET-3D-APL. We observe that methods with higher metrics not only have more valid detections but also have better localization as indicated by higher mLA. We can also verify the assumption of depth errors being a constant percentage of range by checking the consistent mLA values with different range breakdowns.

The results suggest that the evaluation of camera-only detection methods may benefit from the proposed metrics as they quantify the performance in a more fine-grained way.

Method	Metrics	Class				Range		
		All	Vehicle	Pedestrian	Cyclist	[0, 30)	[30, 50)	[50, ∞)
BEVFormer	3D AP (%)	35.3	50.7	22.3	33.0	57.3	23.9	8.7
	LET-3D-AP (%)	70.7	82.9	71.1	58.1	82.0	66.9	50.1
	LET-3D-APL (%)	56.2	68.8	53.2	46.5	65.8	53.7	38.9
	mLA	0.795	0.830	0.748	0.800	0.802	0.803	0.776
FCOS3D-MVDet3D	3D AP (%)	30.3	45.6	16.7	28.5	51.5	17.8	5.7
	LET-3D-AP (%)	66.0	82.1	63.0	53.0	80.2	59.9	36.7
	LET-3D-APL (%)	51.1	66.9	45.0	41.3	62.7	45.5	27.7
	mLA	0.774	0.815	0.714	0.779	0.782	0.760	0.755
CMKD	3D AP (%)	20.9	31.9	12.6	18.3	38.3	11.2	2.9
	LET-3D-AP (%)	51.0	65.6	50.7	36.7	65.3	45.8	25.4
	LET-3D-APL (%)	37.9	50.9	34.9	27.8	49.4	33.4	18.1
	mLA	0.743	0.776	0.688	0.757	0.757	0.729	0.713

Table 2. **Winning methods of the WOD 2022 3D Camera-Only Detection Challenge.** The methods are evaluated on the WOD camera only test set with 80 multi-camera sequences. The results show that proposed LET metrics is suitable for evaluating camera-only 3D detectors. More details of these methods can be found in the leaderboard of the challenge [1].

6. Conclusion

We proposed a novel metric, LET-3D-AP(L) for evaluating camera-only 3D detection methods. The tolerance along the longitudinal axis allows camera-based detections to be associated with the corresponding ground truth bounding boxes despite depth estimation errors. With the longitudinal affinity weighted LET-3D-APL, the detections are rewarded partially for a correct association with ground truth objects. We hope the proposed metrics will help advance the field of camera-only 3D detection by providing a more meaningful indication of method performance.

References

- [1] 2022 waymo open dataset challenge: 3d camera-only detection. <https://waymo.com/open/challenges/2022/3d-camera-only-detection/>.
- [2] Waymo open dataset code repository. <https://github.com/waymo-research/waymo-open-dataset>.
- [3] Garrick Brazil and Xiaoming Liu. M3d-rpn: Monocular 3d region proposal network for object detection. In *ICCV*, 2019.
- [4] Holger Caesar, Varun Bankiti, Alex H. Lang, Sourabh Vora, Venice Erin Liong, Qiang Xu, Anush Krishnan, Yu Pan, Giancarlo Baldan, and Oscar Beijbom. nuscenes: A multimodal dataset for autonomous driving. *arXiv preprint arXiv:1903.11027*, 2019.
- [5] Xiaozhi Chen, Kaustav Kundu, Ziyu Zhang, Huimin Ma, Sanja Fidler, and Raquel Urtasun. Monocular 3d object detection for autonomous driving. In *CVPR*, 2016.
- [6] Mark Everingham, SM Eslami, Luc Van Gool, Christopher KI Williams, John Winn, and Andrew Zisserman. The pascal visual object classes challenge: A retrospective. *IJCV*, 2015.
- [7] Andreas Geiger, Philip Lenz, and Raquel Urtasun. Are we ready for autonomous driving? the kitti vision benchmark suite. In *CVPR*, 2012.
- [8] Alex H Lang, Sourabh Vora, Holger Caesar, Lubing Zhou, Jiong Yang, and Oscar Beijbom. Pointpillars: Fast encoders for object detection from point clouds. In *CVPR*, 2019.
- [9] Tsung-Yi Lin, Michael Maire, Serge Belongie, James Hays, Pietro Perona, Deva Ramanan, Piotr Dollár, and C Lawrence Zitnick. Microsoft coco: Common objects in context. In *ECCV*, 2014.
- [10] Xinzhu Ma, Yinmin Zhang, Dan Xu, Dongzhan Zhou, Shuai Yi, Haojie Li, and Wanli Ouyang. Delving into localization errors for monocular 3d object detection. In *CVPR*, 2021.
- [11] Gregory P Meyer, Ankit Laddha, Eric Kee, Carlos Vallespi-Gonzalez, and Carl K Wellington. Lasernet: An efficient probabilistic 3d object detector for autonomous driving. In *CVPR*, 2019.
- [12] Arsalan Mousavian, Dragomir Anguelov, John Flynn, and Jana Kosecka. 3d bounding box estimation using deep learning and geometry. In *CVPR*, 2017.
- [13] Charles R Qi, Or Litany, Kaiming He, and Leonidas J Guibas. Deep hough voting for 3d object detection in point clouds. In *ICCV*, 2019.
- [14] Cody Reading, Ali Harakeh, Julia Chae, and Steven L Waslander. Categorical depth distribution network for monocular 3d object detection. In *CVPR*, 2021.
- [15] Thomas Roddick, Alex Kendall, and Roberto Cipolla. Orthographic feature transform for monocular 3d object detection. *arXiv preprint arXiv:1811.08188*, 2018.
- [16] Danila Rukhovich, Anna Vorontsova, and Anton Konushin. Imvoxelnet: Image to voxels projection for monocular and multi-view general-purpose 3d object detection. In *WACV*, 2022.
- [17] Shaoshuai Shi, Chaoxu Guo, Li Jiang, Zhe Wang, Jianping Shi, Xiaogang Wang, and Hongsheng Li. Pv-rcnn: Point-

- voxel feature set abstraction for 3d object detection. In *CVPR*, 2020.
- [18] Andrea Simonelli, Samuel Rota Buló, Lorenzo Porzi, Manuel López-Antequera, and Peter Kotschieder. Disentangling monocular 3d object detection. In *ICCV*, pages 1991–1999, 2019.
- [19] Vishwanath A Sindagi, Yin Zhou, and Oncel Tuzel. Mvx-net: Multimodal voxelnet for 3d object detection. In *ICRA*, 2019.
- [20] Pei Sun, Henrik Kretzschmar, Xerxes Dotiwalla, Aurelien Chouard, Vijaysai Patnaik, Paul Tsui, James Guo, Yin Zhou, Yuning Chai, Benjamin Caine, et al. Scalability in perception for autonomous driving: Waymo open dataset. In *CVPR*, 2020.
- [21] Pei Sun, Weiyue Wang, Yuning Chai, Gamaleldin Elsayed, Alex Bewley, Xiao Zhang, Cristian Sminchisescu, and Dragomir Anguelov. Rsn: Range sparse net for efficient, accurate lidar 3d object detection. In *CVPR*, 2021.
- [22] Jonas Uhrig, Nick Schneider, Lukas Schneider, Uwe Franke, Thomas Brox, and Andreas Geiger. Sparsity invariant cnns. In *International Conference on 3D Vision (3DV)*, 2017.
- [23] Tai Wang, Xinge Zhu, Jiangmiao Pang, and Dahua Lin. Fcos3d: Fully convolutional one-stage monocular 3d object detection. In *ICCV*, 2021.
- [24] Yan Wang, Wei-Lun Chao, Divyansh Garg, Bharath Hariharan, Mark Campbell, and Kilian Q Weinberger. Pseudo-lidar from visual depth estimation: Bridging the gap in 3d object detection for autonomous driving. In *CVPR*, 2019.
- [25] Yue Wang, Vitor Campagnolo Guizilini, Tianyuan Zhang, Yilun Wang, Hang Zhao, and Justin Solomon. Detr3d: 3d object detection from multi-view images via 3d-to-2d queries. In *CORL*. PMLR, 2022.
- [26] Bin Xu and Zhenzhong Chen. Multi-level fusion based 3d object detection from monocular images. In *CVPR*, 2018.
- [27] Xingyi Zhou, Dequan Wang, and Philipp Krähenbühl. Objects as points. *arXiv preprint arXiv:1904.07850*, 2019.
- [28] Yin Zhou and Oncel Tuzel. Voxelnet: End-to-end learning for point cloud based 3d object detection. In *CVPR*, 2018.